Journal of Coastal Research	00	0	000–000	Coconut Creek, Florida	Month 0000

TECHNICAL COMMUNICATIONS

www.cerf-jcr.org

Deriving Rich Coastal Morphology and Shore Zone Classification from LIDAR Terrain Models

Wiebe Nijland[†‡]*, Luba Y. Reshitnyk[‡], Brian M. Starzomski[‡§] John D. Reynolds[‡††], Chris T. Darimont[†‡], and Trisalyn A. Nelson[†‡]

[†]Department of Geography
University of Victoria
British Columbia, Canada

[‡]Hakai Institute,
Calvert Island
British Columbia, Canada

[§]School of Environmental Studies
University of Victoria
British Columbia, Canada

[††]Department of Biological Sciences
Simon Fraser University
British Columbia, Canada

ABSTRACT

Nijland, W.; Reshitnyk, L.Y.; Starzomski, B.M.; Reynolds, J.D.; Darimont, C.T., and Nelson, T.A., 2016. Deriving rich coastal morphology and shore zone classification from LIDAR terrain models. *Journal of Coastal Research,* 00(0), 000–000. Coconut Creek (Florida), ISSN 0749-0208.

Comprehensive mapping of shore-zone morphology supports evaluation of shore habitat, monitoring of environmental hazards, and characterization of the transfer of nutrients between marine and terrestrial environments. This article shows how rich shore-zone morphological metrics can be derived from LIDAR terrain models and evaluates the application of LIDAR to classify shore-zone substrates. The utility of LIDAR methods was tested in comparison with the current best-practice method of photo interpretation (*i.e.* the BC ShoreZone system) on Calvert Island, British Columbia, Canada. Wider applications are considered. Indicators of shore-zone morphology (*i.e.* slope, width, roughness, backshore elevation) were calculated from LIDAR terrain models for regularly spaced transects perpendicular to the coastline. A combination of boosted regression-tree modeling and direct-rule application was used to classify the shore-zone morphology according to the British Columbia (BC) ShoreZone system. Classification accuracy was assessed against existing ShoreZone classification data. Shore-zone substrate was classified from LIDAR-derived morphometric indicators with 90% accuracy (five classes). A full classification, which combined substrate with shore width and slope, results in lower correspondence (40%; 25 classes) when compared with ShoreZone classes. Differences can likely be attributed, in part, to variation in spatial resolution of elevation-based methods and photo interpretation. It is concluded that LIDAR data can be used to support characterization of shore-zone morphology. Differences in processing and interpretation cause a low direct correspondence with the current image-based classification system, but LIDAR has the advantage of higher resolution, rich terrain information, speed, and an objective and repeatable method for monitoring future change in coastal environments.

ADDITIONAL INDEX WORDS: *British Columbia, coast, digital elevation model, substrate.*

www.JCRonline.org

INTRODUCTION

The marine–terrestrial interface (the *shore zone*) is one of the most dynamic and important habitats in coastal ecosystems. Shore-zone morphology influences the interaction between marine and terrestrial environments (Bakker *et al.,* 2015; Heerhartz *et al.,* 2014; Orr *et al.,* 2005), and the intertidal zone is the foraging ground for many species that benefit from added food availability provided by the transition from ocean to land (Carlton and Hodder, 2003; Hori and Noda, 2001). Organic material from seaweed wrack also functions as a spatial-nutrient subsidy from the productive ocean to the often nutrient-limited land. Processes that transfer nutrients from the ocean to the shore are important for coastal systems, especially small islands and regions with poor soil, which tend to lack other sources of nutrients and support less biodiversity (Anderson, Wait, and Stapp, 2008; Polis and Hurd, 1996; Trant *et al.,* 2016). Detailed mapping of shore-zone morphology is necessary to further the understanding of these nutrient subsidies. Further, such mapping can support evaluation of the effects of environmental hazards, such as oil or other contaminant spills (Haggarty *et al.,* 2003; Irvine, Mann, and Short, 2006), and provide important baseline information on habitat conditions for monitoring invasive species (such as some seaweed species; Harney, 2008) or populations of at-risk species (including shorebirds; Rickbeil *et al.,* 2014).

Currently, the best-available shore-zone data on the east Pacific coast are from the British Columbia (BC) ShoreZone classification system, which is based on expert classification of oblique aerial images (Howes, Harper, and Owens, 1994; Howes, 2000). Classification of natural coastlines is based principally on shore-zone substrate, width, and slope. The average shore unit length in these classifications in BC is around 500 m, which limits application on smaller islands and

DOI: 10.2112/JCOASTRES-D-16-00109.1 received 10 June 2016; accepted in revision 9 August 2016; corrected proofs received 29 September 2016; published pre-print online 17 November 2016.
*Corresponding author: uvic@wiebenijland.nl

in complex landscapes. In more recent shore-zone mapping projects in Alaska, units are smaller and average around 300 m (Harper and Morris, 2014). Although the ShoreZone system does include characterization of the backshore and shallow, subtidal zones, these fields are not currently filled for most of the BC coast. The backshore is relevant with respect to the permeability of the coast to nutrients (*i.e.* how easily nutrient-rich materials, such as seaweeds, are deposited into terrestrial habitats, such as the nearshore forest). The low intertidal and shallow, subtidal zones may act as important sources of marine wrack because of the presence of seagrass or kelp beds (Krumhansl and Scheibling, 2012). To improve the utility of the ShoreZone data for understanding ecological processes, such as nutrient transfer, spatial resolution needs to be increased, adding more detail to morphological and backshore characterization.

Airborne laser altimetry has gained traction for coastal systems monitoring during the past two decades (Earlie *et al.,* 2015; Klemas, 2011; Leatherman, 2003; Mason, Gurney, and Kennett, 2000; Sallenger *et al.,* 2003; Wozencraft and Lillycrop, 2003). Laser altimetry provides height data and coastline position on par with the best ground-based methods (Graaf *et al.,* 2003; Sallenger *et al.,* 2003; Stockdon *et al.,* 2002). Moreover, measurements are repeatable and relatively affordable (Mason, Gurney, and Kennett, 2000; Pawlowski, Brooks, and Oswald, 2002). In the intertidal and shallow, subtidal zone, standard topographic LIDAR are integrated with bathymetric LIDAR, which uses powerful green lasers to detect the bottom surface through the water column (Quadros, Collier, and Fraser, 1998; Wozencraft, 2010; Wozencraft and Lillycrop, 2003). High spatial resolution LIDAR data have proven to be powerful in many applications, including terrestrial and marine ecosystem mapping (Smeeckaert *et al.,* 2013), habitat modeling (Yamamoto *et al.,* 2012), and tracking changes in coastal and dune morphology (Heathfield and Walker, 2015; Saye *et al.,* 2005; Zarnetske *et al.,* 2015).

A challenge in the application of laser scanning for shore-zone classification is extracting data on substrate type and seaweed assemblages, which are commonly characterized from images and essential to the BC ShoreZone classification system (Howes, Harper, and Owens, 1994). Substrate and biological cover are not directly measured by LIDAR but may be derived from LIDAR derivatives to obtain a more-complete characterization without involving additional data acquisition. Coastline position and shore-zone width can be defined from either images or elevation data, but the definitions are not necessarily compatible (Moore, 2000; Ruggerio *et al.,* 2013).

LIDAR applications often focus on sedimentary coastlines, in which shore morphology is highly dynamic, and in populated areas, with acute coastal-management concerns (Graaf *et al.,* 2003; Leatherman, 2003; Sallenger *et al.,* 2003). However, LIDAR technology shows promise to improve the resolution of existing shore-zone data on Canada's remote Pacific Coast, where increased resource exploitation and transportation interest are focused. Further, LIDAR data can enhance coastline maps through rich morphological information and continuous height measurements. Continuous-scale elevation data are specifically relevant in monitoring the response and vulnerability of a coastline to sea-level change (Schlacher and Schoeman, 2008).

The aim of this study was to use the available LIDAR data to map and characterize the shore zone. The utility of LIDAR data to characterize mixed or rocky shores was demonstrated, and the ability to classify shore-zone substrate from morphological metrics was evaluated. Extraction of shore-zone morphology from high-resolution elevation data required the definition of morphological metrics that were relevant in the coastal context. Before the rapid advance of LIDAR technology, elevation models with sufficient detail—and consequently morphological derivatives—were not available over large areas. Accordingly, the following three objectives were covered: (1) develop objective methods to delineate the shore zone from LIDAR data, (2) define shore-zone morphological metrics in shore-normal and alongshore direction, and (3) evaluate the applicability of metrics for shore-zone substrate prediction. The rapid increase of LIDAR data availability, for example, through the United States Interagency Elevation Inventory (http://coast.noaa.gov/inventory) in the United States (DOC *et al.,* 2016) underscores the importance of developing methods to create value-added information from LIDAR.

METHODS

Shore-perpendicular transects were derived from LIDAR elevation models, starting just inside the vegetation boundary and crossing the shore zone. Morphological metrics were calculated for the transects and were used to classify substrate and ShoreZone class. The LIDAR-derived classification was evaluated against a subset of the existing BC ShoreZone data set.

Study Area

Calvert Island lies on the central coast of British Columbia, Canada, in the NE Pacific Ocean (Figure 1). The area has a temperate marine climate and high average yearly rainfall of more than 2000 mm. The area is located in the Coastal Western Hemlock biogeoclimatic zone (Pojar, Klinka, and Meidinger, 1987), with productive coniferous forest composed of western hemlock (*Tsuga heterophylla* [Raf.] Sarg.), Sitka spruce (*Picea sitchensis* [Bong.] Carr.), and western redcedar (*Thuja plicata* Donn ex D. Don) as the dominant vegetation. On areas with shallow soils and poor drainage, bogs and bog forests are common. The area has a long history (*i.e.* 13,000 y or more) of human use, which concentrates in the coastal margin and has resulted in the presence of clam gardens, fish traps, and altered habitation sites (Lepofsky and Caldwell, 2013; McLaren, Rahemtulla, and Fedje, 2015; Trant *et al.,* 2016). The shoreline elevation (sea level) has been very constant in the past 14,000 y because the island is positioned on a postglacial sea-level hinge (McLaren *et al.,* 2014), facilitating a uniquely long history. The shores have a mix of bedrock and embayed sedimentary beaches on exposed locations and some areas with dune-backed beaches or sand and mudflats. Tides are semidiurnal with a range of 3–5 m (Canada Department of Fisheries and Oceans, 2015).

The BC ShoreZone Data Set

The ShoreZone data set is the most comprehensive shore morphology data set currently available for the North

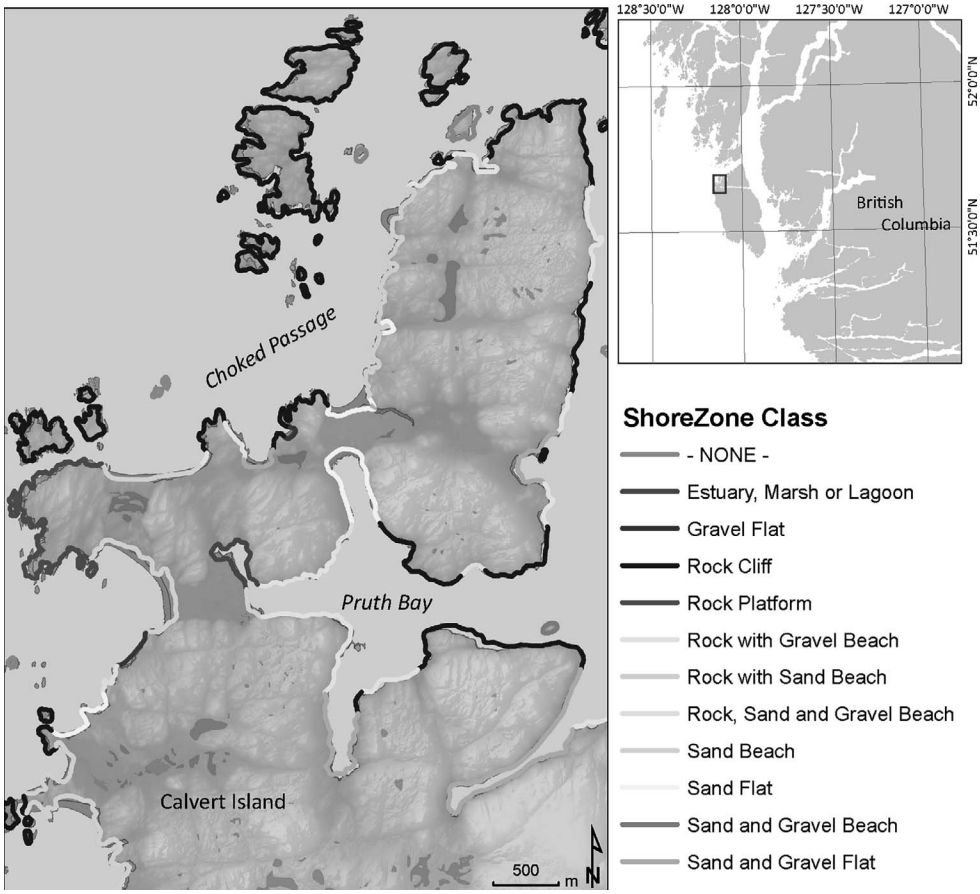

Figure 1. Study area map showing the shore zone types as recorded in the BC ShoreZone data set and extent of the study area. (Color for this figure is available in the online version of this paper.)

American Pacific coast. The mapping procedure uses low-altitude, oblique aerial photography and videography, which are interpreted by an expert to assign habitat classes and to identify specific objects of interest (Howes, Harper, and Owens, 1994; Howes, 2000). The method has been further developed to include estuary systems (Howes, Morris, and Zacharias, 1999) and permafrost-dominated coastlines in the northern regions (Harper and Morris, 2014). The ShoreZone mapping has been completed for 85% of Alaska and all of Oregon, Washington, and British Columbia and is publicly accessible at http://www.shorezone.org. A similar mapping system is currently applied on parts of the Canadian north coasts (Wynja *et al.,* 2015). The most-recent applications meet mapping standards at 1:10,000 or better scales and attribute each coastal section with an extensive set of observations and parameters in addition to habitat classes. Available data for the BC coast have a 1:40,000 reference scale for large parts, which means that, especially small islands and topographically variable sections of the coast, are poorly resolved.

The original shore-zone habitat classification system (Howes, Harper, and Owens, 1994) had 34 classes, which were hierarchically ordered by substrate (rock, gravel, sand, and mixed types), intertidal zone width (<30 m, >30 m), and intertidal zone slope (<5°, 5–20°, >20°), with independent classes for estuaries, human-made shores, and current-dominated channels. Exposure was also recorded from fetch-length calculations, and it incorporates seaweed and other biological indicators, as well as physical descriptors, including tidal range, shore-normal direction, and shoreline stability. All information is recorded to coastline sections that are delineated from an existing base map, in most cases, nautical charts. Human-made shorelines and channels are excluded because they are rare in the study area, leaving 31 possible classes. The combined shore length of Calvert Island and adjacent islets is 266 km, as measured by the sum of arc lengths in the ShoreZone database, and represents 25 habitat classes. Most of the coast is characterized as rock ramp or rock cliff, but sand beaches, sand and gravel flats, and mixed rock and sediment types are common as well. This study focused on the NW corner of Calvert Island and adjacent islets (Figure 1). This area has a broad cross-section of shore-zone habitats, making it ideal as a testing area.

LIDAR Data and Preparation

Discrete return airborne scanning LIDAR was acquired on 15 August 2012 by Terra Remote Sensing Inc. (Sidney, BC,

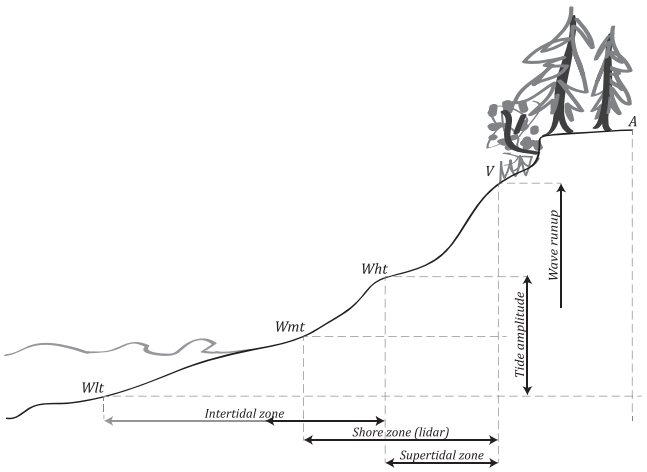

Figure 2. Coastal profile illustrating different zones on the shore. *Wlt* = low-tide elevation, *Wmt* = mean water level, *Wht* = high-tide elevation, *V* = vegetation boundary, *A* = transect projection baseline. Definition of the shore zone by different elevations or boundaries may lead to differences in shore-zone width and other characteristics.

Canada). LIDAR was collected from 1150 m above ground level (AGL) at 100 KHz, with a maximum scan angle of 26°. The resulting point data have an average density of 2 points m^{-2} with a vertical accuracy of 15 cm. A digital terrain surface was generated from classified ground returns using triangular, irregular network interpolation and was rasterized at a spatial resolution of 1.0 m.

Shore-Zone Delineation

An obvious way to delineate the shore zone from elevation data is to use the maximum astronomical tide amplitude and extract the upper and lower levels to define the shore-zone boundaries (Figure 2). This is in line with the definition of the *shore zone* as the intertidal range (Howes, Harper, and Owens, 1994). However, in practice, the shore zone is judged from visual marks like seaweed color bands (biobands) or the flood mark. These indicators allow for flexibility in interpretation and are influenced by still-water levels as well as wave run-up or other local conditions. Biobands are not readily detectable in LIDAR data because color is not recorded, and the footprint does not support resolving the texture of seaweeds. The terrestrial vegetation edge is, therefore, adopted as an alternative upper boundary to the shore zone (Figure 2). This boundary does include the splash zone on the shore but may result in a better-equivalent shore delineation than an elevation-based definition. In coastal areas with dunes, this boundary is called the *erosional threshold elevation* (Heathfield, Walker, and Atkinson, 2013). To find the best-equivalent shore-zone delineation, the width and slope of the shore zone derived by different methods is compared with the width and slope of their assigned classes in the ShoreZone data set (n = 1213 transects). The classification accuracy between the ShoreZone data and different LIDAR-derived shore delineations was evaluated based on the confusion matrix and Cohen's κ (Cohen, 1960). κ is a commonly used statistic in classified (categorical) data that compares agreement between classifiers to chance levels. Values of κ can be between –1 and 1, where 0 indicates agreement no better than chance, >0.4 indicates fair agreement, >0.75 is good or very good agreement, and 1 is perfect agreement (Landis and Koch, 1977; Monserud and Leemans, 1992).

Processing Coastline Morphology

Terrain attributes were extracted on regularly spaced transects, perpendicular to the coastline (shore normal). A transect every 20 m balanced detail with computation efficiency and variability of the shore zone, but the method allowed for any transect spacing down to the primary resolution of the elevation data (1 m). Transects were based on a generalized shore direction and the need to intersect with both the vegetation boundary and the waterline to enable extraction of all relevant shore-zone attributes. To generalize the transect directions, the shore-normal direction was calculated from a baseline that intersects the shore line 100 m on each side of the transect. The process is similar to the Digital Shoreline Analysis System (DSAS) (Himmelstoss, 2009) but uses the landside boundary, buffered by 10 m inland as the baseline, eliminating the need to hand-draw a baseline (Figure 3). For narrow coves or other areas in which the projected shore-normal transect did not overlap with the ocean, transects were drawn as the shortest connector between the baseline and the ocean. In addition to the perpendicular, the profile-turning angle of the baseline in the *x*–*y* plane was also extracted to represent the orthographic shape of the coast (strait coast *vs*. bay *vs*. point). From the shore-normal transects, morphological metrics, including the transect-bearing, width, and slope of different shore zones were calculated, as well as the elevation of the backshore boundary (Table 1). Transect lines were also used to extract morphological indicators, calculated from the raster elevation model. Raster digital elevation model (DEM) derivatives were calculated in ENVI 4.8 using a 5 × 5 cell kernel, except for roughness, which was derived on a 3 × 3 or 9 × 9 cell kernel (Wood, 1996). Table 1 lists all the derived metrics with more-detailed definitions, units, and typical ranges in the area.

Shore-Zone Classification

Boosted regression trees were used to build a predictive model of the ShoreZone substrate classes based on morphological metrics available from LIDAR. Boosted regression trees are highly flexible because they accept both continuous and classified variables and are able to fit nonlinear relations and interactions between parameters (Elith, Leathwick, and Hastie, 2008). The classifier was trained on a subset of available ShoreZone data, which was selected and verified for substrate type with field observations and high-resolution photo interpretation (~2500 m coastline, covering 1212 transects). The same selection was used for evaluation of shore-zone delineation. From the reference data, training (n = 500) and validation (n = 100) samples were independently drawn with an equal number of observations for each of the substrate classes. The validation sample was used to fill a confusion matrix (Stehman, 1997) for predicted *vs*. ShoreZone substrate types.

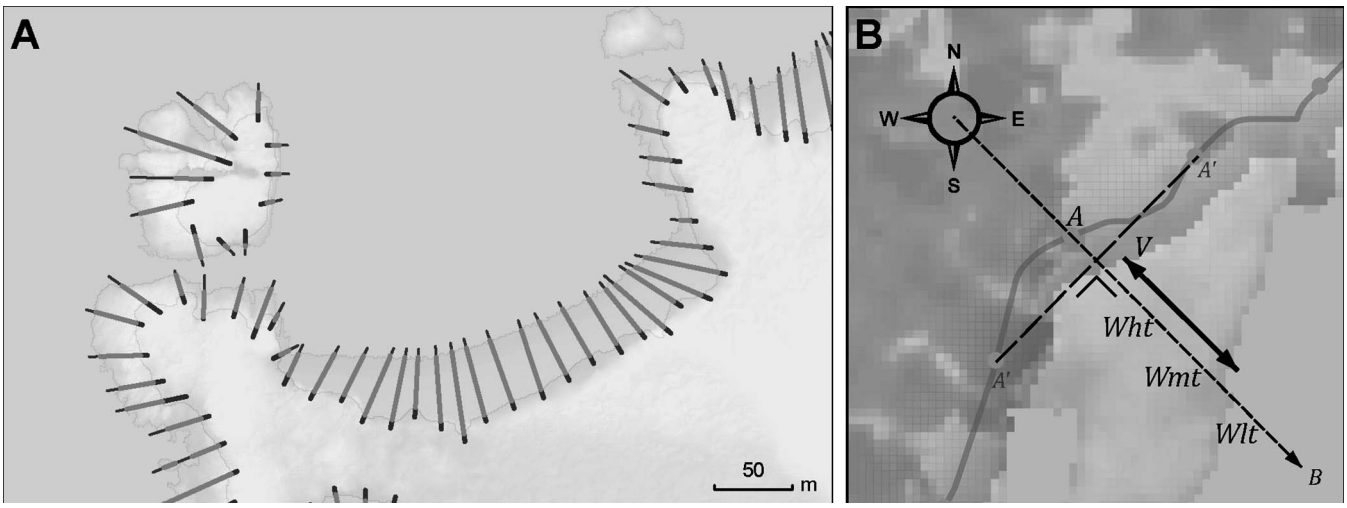

Figure 3. (A) Map of an example coastline with morphology transects. (B) Example morphology transect. A-A' = transect projection baseline, B = transect end, *Wlt* = low-tide elevation, *Wmt* = mean water level, *Wht* = high-tide elevation, V = vegetation boundary. The two-sided arrow indicates the shore-zone width. (Color for this figure is available in the online version of this paper.)

RESULTS

Shore-morphology transects were created on approximately 7800 m of coastline. Of the projected transects 84% were generated by perpendicular projection. The remaining 16% were projected as the shortest path to the waterline because perpendicular projection did not produce a transect that crossed both the vegetation boundary and the waterline. Mean transect length (from the baseline to the datum waterline) was 33.5 m, and the maximum length was 156.1 m. Mean transect slope was 19.1°.

In the LIDAR-derived shore metrics, there are several ways to define the shore boundaries that produce different shore widths and slopes. Comparison of ShoreZone class width and LIDAR-derived widths using tidal elevations or the vegetation edges (Figure 4) reveals greater range and difference among the classes for the vegetation-based definitions than for the elevation-based definitions. Using the elevation-based defini-

Table 1. *Terrain metrics used as shore-zone morphology indicators, with names, formula or description, typical range, and unit. A = transect baseline, asl = above sea level, B = transect end, NAB = azimuth of line AB to geographic North, RMSE = root mean square error, Wlt = low-tide elevation, Wht = high-tide elevation, V = vegetation boundary, δ_z = elevation difference (Figures 2 and 3).*

Transect metrics	Description	Typical Range	Unit
Transect bearing	$\angle NAB$	0–360	°
Intertidal zone width	$\lvert W_{lt} - W_{ht}\rvert$	1–100	m
Supertidal zone width	$\lvert V - W_{ht}\rvert$	1–100	m
Shore zone width	$\lvert V - W_{lt}\rvert$	1–200	m
Backshore boundary elevation	*Elevation (V)*	0–40	m asl
Baseline elevation	*Elevation (A)*	0–50	m asl
Intertidal zone gradient	$\tan^{-1}\frac{\delta_z(W_{lt}W_{ht})}{\lvert W_{lt}-W_{ht}\rvert}\frac{180}{\pi}$	1–50	°
Supertidal zone gradient	$\tan^{-1}\frac{\delta_z(W_{ht}V)}{\lvert V-W_{ht}\rvert}\frac{180}{\pi}$	1–90	°
Shore zone gradient	$\tan^{-1}\frac{\delta_z(W_{lt}V)}{\lvert V-W_{lt}\rvert}\frac{180}{\pi}$	1–90	°
Raster metrics	Raster derivatives calculated in ENVI 4.8 according to Wood (1996)		
Shore zone median aspect	Compass direction of maximum gradient	0–360	°
Shore zone average elevation	DEM elevation	0–20	m asl
Intertidal zone average gradient	Average DEM rate of change	0–75	°
Shore zone average gradient	Average DEM rate of change	0–75	°
Shore zone maximum gradient	Maximum DEM rate of change	4–90	°
Shore zone roughness 3 × 3 kernel	Root mean square difference between DEM and quadratic fit	0–4	m
Shore zone roughness 9 × 9 kernel		1–150	m
Profile convexity average	Curvature in z plane	−3 to 3	m/m
Plan convexity average	curvature in x–y plane	−3 to 3	m/m
Backshore >1m vegetation average height	Average maximum LIDAR point height above the surface for cells with >1 m points	1–40	m
Backshore elevation RMSE	Root mean square difference between DEM and quadratic fit	1–150	m
Backshore elevation maximum	Maximum DEM between $V - A$	1–50	m
Orthographic metrics			
Baseline turning angle	*External* $\angle A_{-100}A_{+100}$	0–360	°

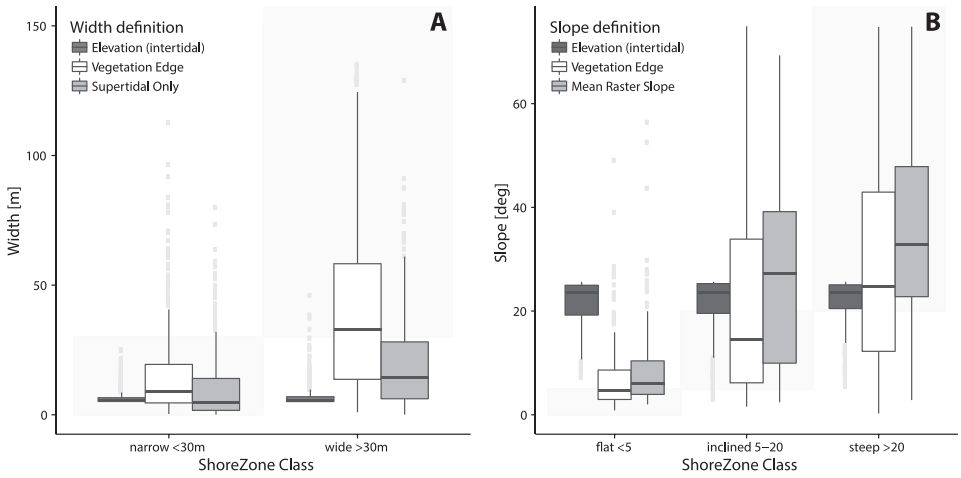

Figure 4. Comparison between ShoreZone width (A) and slope (B) classes and LIDAR-derived morphological metrics. The distribution of LIDAR-derived shore width and slope for transects on each of the ShoreZone class width and slope is shown as box plots (box is quartiles, whiskers are 2.5 and 97.5 percentiles). Background shading indicates the ShoreZone class range. Defining the shore zone by vegetation edge has the closest match between both data sources.

tion for classification produces κ values near 0 ($\kappa = 0.01$). The vegetation edge has higher, but still marginal, accuracy ($\kappa = 0.20$). For slope, the result was similar: the elevation-based definition separated the classes very poorly ($\kappa = 0.01$). Including the shore zone to the vegetation edge gave better results, with transect gradient performing better ($\kappa = 0.17$) than mean raster slope ($\kappa = 0.10$).

LIDAR methods classified substrate type from the morphological parameters for five substrate classes (rock, rock and sediment, gravel, sand, and mud) with an overall accuracy of 90% (Table 2). The strongest predictor variable was roughness (9×9 kernel), with shore slope and width variables being the next most important (Figure 5). Curvature, vegetation height, and shore-turning angle had low variable importance, indicating they were weakly related to shore-zone substrate. The most commonly confused class was the mixed rock and sediment, which was confused with either rock or sand.

A classification equivalent to the ShoreZone system was created from the LIDAR metrics, combining the predicted substrates with shore-zone slope and width, the three defining characteristics of the ShoreZone system (Howes, Harper, and Owens, 1994). Table 3 shows the confusion matrix for this classification against the ShoreZone classes in the training data set ($n = 500$): the overall accuracy was modest at 41%. Much of the confusion occurred between similar classes, such as rock ramp and rock cliff, or mixed types, such as rock and with narrow beach. Pure classes like sand beach and mud flat had greater accuracy.

DISCUSSION

This article demonstrates the utility of LIDAR elevation data to describe shore-zone morphology and to classify shore-zone habitat. Classification of substrate types from morphological metrics was successful with an accuracy of 90% (Table 2). However, when the LIDAR-derived shore morphology was used to generate a detailed classification, equivalent to the BC ShoreZone system, correspondence was much lower at 41% (Table 3).

Low correspondence between the LIDAR-derived shore-zone classification and the image interpretation–based classification of the ShoreZone system may be partly attributed to the fundamental differences between these systems, although differences are also caused by inaccuracies in either system. The main difference is the primary spatial unit of attribution, which is a shore-perpendicular transect in the introduced system and a linear section of coastline in the BC ShoreZone system. The ShoreZone system has a larger primary unit (on average 500 m of coastline in the study area), whereas in the

Table 2. *Confusion matrix for the predicted shore zone substrate vs. ShoreZone validation sample. Overall accuracy: 90%.*

	Reference					
Prediction	Gravel	Mud	Rock	Rock and Sediment	Sand	Percentage (%)
Gravel	18	0	0	0	0	100.0
Mud	1	20	0	0	0	95.2
Rock	1	0	17	1	0	89.5
Rock and sediment	0	0	3	16	1	80.0
Sand	0	0	0	3	19	86.4
Total (%)	90.0	100.0	85.0	80.0	95.0	
Accuracy (%)	90.0					
κ	0.88					
Training accuracy (%)	95.4					

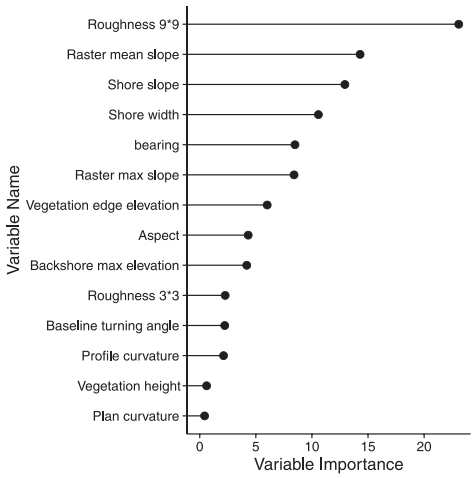

Figure 5. Relative variable importance for the generalized boosted regression prediction model of shore-zone substrate (for variable descriptions, refer to Table 1). Variable importance shows the relative variable importance and sums to 100. Roughness and slope are the most influential variables for substrate prediction.

analysis, the transects are spaced 20 m apart, leading to a greater degree of mixed shore types and less variability in slopes and widths because of aggregation of short units into larger sections.

The accuracy of the ShoreZone mapping system is influenced by a number of factors: the geomorphology and complexity of the coast, the quality of the imagery, the quality of the available shoreline base map, and the experience of the mapper (Harper and Morris, 2014). Harper and Morris (2014) summarized a number of verification studies conducted around Victoria, British Columbia, and Sitka, Alaska, indicating a correspondence of 80% between mapping on the ground and aerial data. Intertidal widths estimated matched ground verification in 63% of the units, with an underestimation bias for aerial mapping. The training and validation units taken from the BC ShoreZone data set in this study were verified on the ground and from high-resolution images to ensure accuracy (56% of the coastline was retained). In this process, some highly ambiguous, misclassified, and poorly resolved shore units are excluded. Confidence in the substrate accuracy of the ShoreZone units used in this study was high, but slopes or widths were not verified other than by comparison to the LIDAR data.

The main sources of error in the LIDAR-based shore classification are in the delineation of the shore-zone boundaries, both on the land and the ocean side. To characterize the shore zone, its extent must first be defined. In interpreted systems, the extent of the shore zone is derived from visible cues like the flood mark, water level at photo acquisition, and seaweed assemblages on the shoreline (Harper and Morris, 2014; Howes, Harper, and Owens, 1994). LIDAR provides high-precision height measurements, allowing for a direct definition of tidal levels in terms of elevation. Adopting a fully elevation-based definition of the shore zone, calculated to the high-tide level, not accounting for wave run-up or other factors, leads to a poor delineation of the shore zone (Figure 4). Terrestrial vegetation marks a transition from ocean and wave–dominated processes to terrestrial processes and, therefore, provides a natural and process-based shore-zone boundary (Heathfield, Walker, and Atkinson, 2013). Inclusion of the super tidal area results in better separation between ShoreZone class, width, and slope. Shore-zone delineation based on LIDAR-derived, high-tide elevation can be difficult on sedimentary coasts because of the dynamic beach heights, depending on tides and storms. Accordingly, Moore (2000) recommended using the top edge of a bluff or dune as a shore-line proxy. Our use of the terrestrial vegetation as the shore-zone boundary was consistent with that of Moore (2000) recommendation.

LIDAR data collected for terrestrial applications often have limited spatial extent on the marine side of the shore zone, being limited to tide elevations at the time of data acquisition. Although LIDAR data allow for use in the upper parts of the shore zone, utility for the lower parts of the shore are improved with purposeful acquisitions coinciding with low tides. Airborne LIDAR data do allow timing acquisitions with low tide but at an increase in operating cost (Wulder *et al.,* 2008). The

Table 3. *Confusion matrix of LIDAR-predicted classes* vs. *ShoreZone data set; class numbers correspond to the BC ShoreZone definitions (Howes, Harper and Owens, 1994), Overall accuracy: 41%.*

		Modeled													
Shore zone		1	2	3	4	5	11	12	13	14	21	22	27	29	
Rock ramp, wide	1	5.0		2.0	0.3	1.2									0.66
Rock platform, wide	2	1.8	0.0	0.6		0.6									—
Rock cliff	3	6.4		5.3	3.8	0.6			0.3						0.67
Rock ramp, narrow	4			0.6	0.6										0.53
Rock platform, narrow	5					0.0									0.50
Ramp with beach, wide	11	0.3		1.5	0.6	0.3	0.6	1.8	0.6	1.2	5.0		7.0	1.2	0.91
Platform with beach, wide	12			0.3	0.3			2.9		0.9	0.3		2.9		0.77
Cliff with beach	13	0.3		0.3	0.9				0.0	2.6			0.3	2.6	0.46
Ramp with beach, narrow	14	0.3		0.6	0.6			0.3		4.1			1.2		0.67
Gravel flat	21				0.0					0.0	0.6				0.55
Gravel beach	22				1.8					1.2		0.0		1.5	—
Sand beach	27					0.3			1.8				7.8		0.78
Mud flat	29													5.3	0.75
Total (%)															40.57

ability to time data collections with tides is a marked advantage over other remote-sensing methods, such as satellite imaging, where it is usually not possible to obtain sufficient data-collection opportunities when the orbit, cloud conditions, and tides all need to be favorable. In addition to standard airborne LIDAR systems, LIDAR sensors are now available that can detect nearshore bathymetry through the water column, expanding the elevation data beyond the low-tide level where standard optical-imaging methods do not provide data (Wozencraft, 2010; Wozencraft and Lillycrop, 2003)

Marked differences exist between the extraction of morphological shore-zone information from digital terrain models and classification in the field or with images and a trained interpreter (*e.g.,* Figures 2 and 3). The ShoreZone system segments the shoreline from a base-map product in the homogeneous sections and assigns classes to each section. The terrain-based method in this article used regularly spaced, perpendicular transects along the coastline to extract the elevation data and to derive morphological metrics. An advantage of deriving a wide variety of metrics is that, apart from using them as inputs for a classification system, the metrics are also available individually for analysis or change-detection purposes (Moore, Grayson, and Ladson, 1991). The use of elevation-based morphological characterization in the shore zone follows developments in the soil and vegetation sciences in which terrain analysis is used to predict vegetation patterns (Davis and Goetz, 1990; Nijland *et al.,* 2014), soil attributes (Moore *et al.,* 1993; Moore, Grayson, and Ladson, 1991), and surface hydrology (Nijland *et al.,* 2015; White *et al.,* 2012). Terrain morphology is also used in combination with image interpretation for the mapping of habitat types on the seabed (Nelson *et al.,* 2011)

Where the detection of shore-zone morphology and coastline position in many areas is quickly moving to elevation-based definitions (Graaf *et al.,* 2003; Leatherman, 2003; Mason, Gurney, and Kennett, 2000; Moore, 2000), mapping the north Pacific and northern shores of Canada and the United States still relies heavily on oblique photography and expert interpretation. Current mapping projects are underway in Alaska (Lindeberg, 2014) and northern Canadian waters. This study explores the potential to include terrain information directly into shore monitoring and classification, thereby reducing the costly need for manual photo interpretations. The quantitative nature of elevation-based methods brings a marked advantage in monitoring settings in which a more-objective, quantitative approach to detecting changes is possible.

CONCLUSIONS

This article introduced a method for extracting shore-zone morphology and substrates from high-resolution, LIDAR-derived elevation data. In comparison to the oblique, aerial-image interpretation–based ShoreZone system, the elevation-based method provides greater spatial-resolution information and generates a more-comprehensive collection of morphological metrics, such as shore width, slope, roughness, and turning angle. Classification of substrate from LIDAR is accurate, with 90% correspondence to field and ShoreZone classes, but more confusion occurs when detailed classes based on shore width and slope are compared. Adoption of the proposed methods can result in lowering the cost of the mapping efforts, which would enable shorter repeat cycles. Recent public availability of LIDAR data on most of the U.S. coastline (DOC *et al.,* 2016) underline the relevance of generating added-value products from high-resolution elevation data. The generation of high spatial resolution shore classification and continuous morphology metrics adds value for ecological, sea-level rise, and other studies.

ACKNOWLEDGMENTS

Funding for this project was provided by the Hakai Institute (http://www.hakai.org), as was access to the LIDAR data used in this study. We thank all members of the Hakai 100 Islands team for their support and company during field data collection.

LITERATURE CITED

Anderson, W.B.; Wait, D.A., and Stapp, P., 2008. Resources from another place and time: Responses to pulses in a spatially subsidized system. *Ecology,* 89(3), 660–670.

Bakker, J.P.; Nielsen, K.J.; Alberti, J.; Chan, F.; Hacker, S.D.; Iribarne, O.O.; Kuijper, D.P.J.; Menge, B.A.; Schrama, M., and Silliman, B.R., 2015. Bottom-up and top-down interactions in coastal interface systems. *In:* Hanley, T.C. and La Pieree, K.J. (eds.), *Trophic Ecology: Bottom–Up and Top–Down Interactions across Aquatic and Terrestrial Systems*. Cambridge, U.K.: Cambridge University Press pp. 157–200.

Canada Department of Fisheries and Oceans, 2015. *Canadian Tide and Current Tables*. Ottawa Ontario: Department of Fisheries and Oceans.

Carlton, J.T. and Hodder, J., 2003. Maritime mammals: Terrestrial mammals as consumers in marine intertidal communities. *Marine Ecology Progress Series,* 256, 271–286.

Cohen, J., 1960. A coefficient of agreement for nominal scales. *Educational and Psychological Measurement,* 20(1), 37–46.

Davis, F.W. and Goetz, S., 1990. Modeling vegetation pattern using digital terrain data. *Landscape Ecology,* 4(1), 69–80.

DOC; NOAA; NOS, and OCM (Department of Commerce; National Oceanic and Atmospheric Administration; National Ocean Service, and U.S. Department of Commerce), 2016. *United States Interagency Elevation Inventory (USIEI)*. Charleston, South Carolina: NOAA.

Earlie, C.S.; Masselink, G.; Russell, P.E., and Shail, R.K., 2015. Application of airborne LIDAR to investigate rates of recession in rocky coast environments. *Journal of Coastal Conservation,* 19(6), 831–845.

Elith, J.; Leathwick, J.R., and Hastie, T., 2008. A working guide to boosted regression trees. *Journal of Animal Ecology,* 77(4), 802–813.

Graaf, H.J.C. de; Elberink, S.J.O.; Bollweg, A.E.; Brügelmann, R., and Richardson, L.R.A., 2003. *Inwinning droge JARKUS profielen langs Nederlandse kust. Ministerie van Verkeer en Waterstaat, Rapportnummer*. Den Haag, Netherlands: Rijkswaterstaat publication, *AGI-GAM-2003-40*.

Haggarty, D.; Mccorquodale, B.; Johannessen, D., and Levings, C., 2003. *Marine Environmental Quality in the Central Coast of British Columbia, Canada: A Review of Contaminant Sources, Types and Risks*. Sidney, British Columbia: Fisheries and Oceans Canada *Canadian Technical Report of Fisheries and Aquatic Sciences Report 2507,* 165p.

Harney, J., 2008. *Modeling Habitat Suitability for the Invasive Salt Marsh Cordgrass* Spartina *Using ShoreZone Coastal Habitat Mapping Data in Southeast Alaska, British Columbia, and Washington State*. Sidney, British Columbia: Coastal & Ocean Resources Inc. *Project 2008-06*.

Harper, J.R. and Morris, M.C., 2014. *Alaska ShoreZone Coastal Habitat Mapping Protocol*. Seldovia, Alaska: Bureau of Ocean Energy Management.

Heathfield, D.K. and Walker, I.J., 2015. Evolution of a foredune and backshore river complex on a high-energy, drift-aligned beach. *Geomorphology,* 248, 440–451.

Heathfield, D.K.; Walker, I.J., and Atkinson, D.E., 2013. Erosive water level regime and climatic variability forcing of beach-dune systems on south-western Vancouver Island, British Columbia, Canada. *Earth Surface Processes and Landforms,* 38(7), 751–762.

Heerhartz, S.M.; Dethier, M.N.; Toft, J.D.; Cordell, J.R., and Ogston, A.S., 2014. Effects of Shoreline Armoring on Beach Wrack Subsidies to the Nearshore Ecotone in an Estuarine Fjord. *Estuaries and Coasts,* 37(5), 1256–1268.

Himmelstoss, E., 2009. DSAS 4.0 Installation instructions and user guide. *In:* Thieler, E.R.; Himmelstoss, E.A.; Zichichi, J.L., and Ergul, A. *Digital Shoreline Analysis System (DSAS) version 4.0—An ArcGIS Extension for Calculating Shoreline Change*. Reston, Virginia: U.S. Geological Survey, *Open-File Report 2008-1278*, 79p.

Hori, M. and Noda, T., 2001. Spatio-temporal variation of avian foraging in the rocky intertidal food web. *Journal of Animal Ecology,* 70(1), 122–137.

Howes, D.; Morris, M., and Zacharias, M., 1999. *British Columbia Estuary Mapping System*. Victoria, British Columbia: Province of British Columbia Resources Inventory Committee, 70p.

Howes, D., 2000. *BC Biophysical Shore-Zone Mapping System—A Systematic Approach to Characterize Coastal Habitats in the Pacific Northwest*. Victoria: British Columbia Land Use Coordination Office, 11p.

Howes, D.; Harper, J., and Owens, E., 1994. *Physical Shore-Zone Mapping System for British Columbia*. Victoria, British Columbia: BC Ministry of Environment Lands and Parks, 71p.

Irvine, G. V; Mann, D.H., and Short, J.W., 2006. Persistence of 10-year old Exxon Valdez oil on Gulf of Alaska beaches: The importance of boulder-armoring. *Marine Pollution Bulletin,* 52(9), 1011–1022.

Krumhansl, K.A. and Scheibling, R.E., 2012. Production and fate of kelp detritus. *Marine Ecology Progress Series,* 467, 281–302.

Klemas, V., 2011. Beach profiling and LIDAR bathymetry: An overview with case studies. *Journal of Coastal Research,* 27(6), 1019–1028.

Landis, J.R. and Koch, G.G., 1977. The measurement of observer agreement for categorical data. *Biometrics,* 33(1), 159–174.

Leatherman, S.P., 2003. Shoreline change mapping and management along the US East Coast. *In:* Byrnes, M.R.; Crowell, M., and Fowler, C. (eds.), *Shoreline Mapping and Change Analysis: Technical Considerations & Management Implications*. *Journal of Coastal Research*, Special Issue No. 38, pp. 5–13.

Lepofsky, D. and Caldwell, M., 2013. Indigenous marine resource management on the Northwest Coast of North America. *Ecological Processes,* 2(1), 12.

Lindeberg, M.R., 2014. *Alaska ShoreZone Coastal Habitat Mapping Program*. Auke Bay: Alaska Fisheries Science Center, 50p.

Mason, D.C.; Gurney, C., and Kennett, M., 2000. Beach topography mapping: A comparison of techniques. *Journal of Coastal Conservation,* 6(1), 113–124.

McLaren, D.; Fedje, D.; Hay, M.B.; Mackie, Q.; Walker, I.J.; Shugar, D.H.; Eamer, J.B.R.; Lian, O.B., and Neudorf, C., 2014. A post-glacial sea level hinge on the central Pacific coast of Canada. *Quaternary Science Reviews,* 97, 148–169.

McLaren, D.; Rahemtulla, F., and Fedje, D., 2015. Prerogatives, sea level, and the strength of persistent places: Archaeological evidence for long-term occupation of the central coast of British Columbia. *BC Studies: The British Columbian Quarterly,* 187, 155–191.

Monserud, R.A. and Leemans, R., 1992. Comparing global vegetation maps with the kappa statistic. *Ecological Modelling,* 62(4), 275–293.

Moore, I.D.; Gessler, P.; Nielsen, G.A., and Peterson, G.A., 1993. Soil attribute prediction using terrain analysis. *Soil Science Society of America Journal,* 57(2), 443–452.

Moore, I.D.; Grayson, R.B., and Ladson, A.R., 1991. Digital terrain modelling: A review of hydrological, geomorphological, and biological applications. *Hydrological Processes,* 5(1), 3–30.

Moore, L.J., 2000. Shoreline mapping techniques. *Journal of Coastal Research,* 16(1), 111–124.

Nelson, T.A.; Gillanders, S.N.; Harper, J., and Morris, M., 2011. Nearshore aquatic habitat monitoring: a seabed imaging and mapping approach. *Journal of Coastal Research,* 27(2), 348–355.

Nijland, W.; Coops, N.C.; Macdonald, S.E.; Nielsen, S.E.; Bater, C.W.; White, B.; Ogilvie, J., and Stadt, J., 2015. Remote sensing proxies of productivity and moisture predict forest stand type and recovery rate following experimental harvest. *Forest Ecology and Management,* 357, 239–247.

Nijland, W.; Nielsen, S.E.; Coops, N.C.; Wulder, M.A., and Stenhouse, G.B., 2014. Fine-spatial scale predictions of understory species using climate- and LIDAR-derived terrain and canopy metrics. *Journal of Applied Remote Sensing,* 8(1), 083572.

Orr, M.; Zimmer, M.; Jelinski, D.E., and Mews, M., 2005. Wrack deposition on different beach types: Spatial and temporal variation in the pattern of subsidy. *Ecology,* 86(6), 1496–1507.

Pawlowski, R.J.; Brooks, P.D., and Oswald, J.L., 2002. Emerging survey technologies for Alaska's coastal zone. *In:* Miller, K.S., *Cold Regions Engineering: Cold Regions Impacts on Transportation and Infrastructure. Proceedings of the 11th International Conference on Cold Regions Engineering* (Anchorage, Alaska, USA), pp. 605–616.

Pojar, J.; Klinka, K., and Meidinger, D., 1987. Biogeoclimatic ecosystem classification in British Columbia. *Forest Ecology and Management,* 22, 119–154.

Polis, G.A. and Hurd, S.D., 1996. Linking marine and terrestrial food webs: Allochthonous input from the ocean supports high secondary productivity on small islands and coastal land communities. *American Naturalist,* 147(3), 396.

Quadros, N.D.; Collier, P.A., and Fraser, C.S., 1998. Integration of bathymetric and topographic LIDAR: A preliminary investigation. *Proceedings of the International Archives of the Photogrammetry Remote Sensing and Spatial Information Sciences XXXVII part B8* (Beijing, China), pp. 1299–1304.

Rickbeil, G.J.M.; Coops, N.C.; Drever, M.C., and Nelson, T.A., 2014. Assessing coastal species distribution models through the integration of terrestrial, oceanic and atmospheric data. *Journal of Biogeography,* 41(8), 1614–1625.

Ruggerio, P.; Kratzmann, M.G.; Himmelstoss, E.A.; Reid, D.; Allan, J., and Kaminsky, G., 2013. *National Assessment of Shoreline Change: Historical Shoreline Change along the Pacific Northwest Coast*. Reston, Virginia: U.S. Geological Survey, 79p.

Sallenger, A.H.; Krabill, W.B.; Swift, R.N.; Brock, J.C.; List, J.H.; Hansen, M.; Holman, R.A.; Manizade, S.; Sontag, J.; Meredith, A.; Morgan, K.; Yunkel, J.K.; Frederick, E.B., and Stockdon, H.F., 2003. Evaluation of airborne topographic lidar for quantifying beach changes. *Journal of Coastal Research,* 19(1), 125–133.

Saye, S.E.; van der Wal, D.; Pye, K., and Blott, S.J., 2005. Beach—dune morphological relationships and erosion/accretion: An investigation at five sites in England and Wales using LIDAR data. *Geomorphology,* 72(1–4), 128–155.

Schlacher, T. and Schoeman, D., 2008. Sandy beach ecosystems: Key features, sampling issues, management challenges and climate change impacts. *Marine Ecology,* 29(s1), S70–S90.

Smeeckaert, J.; Mallet, C.; David, N.; Chehata, N., and Ferraz, A., 2013. Large-scale classification of water areas using airborne topographic lidar data. *Remote Sensing of Environment,* 138, 134–148.

Stehman, S. V, 1997. Selecting and interpreting measures of thematic classification accuracy. *Remote Sensing of Environment,* 62(1), 77–89.

Stockdon, H.F.; Sallenger, A.H., Jr.; List, J.H., and Holman, R.A., 2002. Estimation of shoreline position and change using airborne topographic LiDAR data. *Journal of Coastal Research,* 18(3), 502–513.

Trant, A.J.; Nijland, W.; Hoffman, K.; Mathews, D.; McLaren, D.; Nelson, T., and Starzomski, B.M., 2016. Intertidal resource use over millennia enhances forest productivity. *Nature Communications*. In press. doi:10.1038/ncomms12491

White, B.; Ogilvie, J.; Campbell, D.M.H.; Hiltz, D.; Gauthier, B.; Chisholm, H.K.; Wen, H.K.; Murphy, P.N.C., and Arp, P.A., 2012. Using the cartographic depth-to-water index to locate small streams and associated wet areas across landscapes. *Canadian Water Resources Journal,* 37(4), 333–347.

Wood, J., 1996. *The Geomorphological Characterisation of Digital Elevation Models*. Leicester, U.K.: University of Leicester, 465p.

Wozencraft, J.M.M., 2010. Requirements for the coastal zone mapping and imaging LIDAR (CZMIL). *In:* Shen, S.S. and Lewis P.E. (eds.), *Proceedings of the SPIE: Algorithms and Technologies for Multispectral, Hyperspectral, and Ultraspectral Imagery XVI* (Orlando FL, USA). Volume 7695, Abstract 760501. Bellingham, Washington: SPIE. doi:10.1117/12.851891

Wozencraft, J.M.M. and Lillycrop, W.J.J., 2003. SHOALS airborne coastal mapping: Past, present, and future. *In:* Byrnes, M.R.; Crowell, M., and Fowler, C. (eds.), *Shoreline Mapping and Change Analysis: Technical Considerations and Management Implications*. *Journal of Coastal Research*, Special Issue No. 38, pp. 207–215.

Wulder, M.A.; Bater, C.C.W.; Coops, N.C.; Hilker, T., and White, J.C., 2008. The role of LiDAR in sustainable forest management. *Forestry Chronicle,* 84(6), 807–826.

Wynja, V.; Demers, A.M.; Laforest, S.; Lacelle, M.; Pasher, J.; Duffe, J.; Chaudhary, B.; Wang, H., and Giles, T., 2015. Mapping coastal information across Canada's northern regions based on low-altitude helicopter videography in support of environmental emergency preparedness efforts. *Journal of Coastal Research,* 31(2), 276–290.

Yamamoto, K.H.; Powell, R.L.; Anderson, S., and Sutton, P.C., 2012. Using LiDAR to quantify topographic and bathymetric details for sea turtle nesting beaches in Florida. *Remote Sensing of Environment,* 125(10), 125–133.

Zarnetske, P.L.; Ruggiero, P.; Seabloom, E.W., and Hacker, S.D., 2015. Coastal foredune evolution: the relative influence of vegetation and sand supply in the US Pacific Northwest. *Journal of the Royal Society Interface,* 12, 20150017.